


## Capillary imbibition in lubricant-coated channels

Sergi G. Leyva <sup>1,2,3</sup> Ignacio Pagonabarraga,<sup>1,2</sup>  
Aurora Hernández-Machado,<sup>1,4</sup> and Rodrigo Ledesma-Aguilar<sup>3</sup>

<sup>1</sup>*Departament de Física de la Matèria Condensada, Universitat de Barcelona, 08028 Barcelona, Spain*

<sup>2</sup>*Universitat de Barcelona Institute of Complex Systems (UBICS),  
Universitat de Barcelona, 08028 Barcelona, Spain*

<sup>3</sup>*School of Engineering, University of Edinburgh, The King's Buildings, Mayfield Road,  
Edinburgh EH9 3JL, United Kingdom*

<sup>4</sup>*Institut de Nanociència i Nanotecnologia, Universitat de Barcelona, 08028 Barcelona, Spain*



(Received 2 December 2022; accepted 27 June 2024; published 18 July 2024)

Capillary imbibition underpins many processes of fundamental and applied relevance in fluid mechanics. A limitation to the flow is the coupling to the confining solid, which induces friction forces. Here we study the effect of coating the solid with a liquid lubricant layer. Using a theoretical framework, we show that for sufficiently small lubricant viscosity, dissipation entirely occurs in the lubricant layer, resulting in a linear growth of the advancing front. We extend our study to forced imbibition, where the same mechanism gives rise to an exponential front growth. This new ability to control multiphase flows in confinement opens new opportunities for flow control in micro and nanofluidic devices.

DOI: [10.1103/PhysRevFluids.9.L072002](https://doi.org/10.1103/PhysRevFluids.9.L072002)

Spontaneous imbibition, an example of capillary filling, occurs when one fluid displaces a second one from a solid porous medium due to its preferential affinity to wet the internal surfaces of the solid. Applications can be found in nanofluidics [1], where elastocapillary forces support the self-assembly of arrays of carbon nanotubes [2]; biophysics, where capillary forces are known to influence protein folding [3–5]; and medical devices, where lateral flows, an example of capillary driven flows, are widely used to detect the presence of a target substance, and set the basis for antigen detection [6,7].

Classical imbibition corresponds to a viscous fluid displacing a gas in a uniform porous medium, where the front position,  $l(t)$ , follows the “slowing-down” growth of Washburn’s law,  $l(t) \propto t^\alpha$ , with  $\alpha = 1/2$  [8]. Understanding and controlling the exponent  $\alpha$  is therefore of both fundamental and practical interest. Pradas *et al.* [9,10] and Queralt *et al.* [11] showed that the exponent can be lowered to  $\alpha < 1/2$  by introducing disorder in the channel topography. On the other hand, Primkulov *et al.* [12] reported a larger exponent  $\alpha = 1$ , but lower imbibition speed, by capping the front with a slug of a viscous oil.

What happens if the solid walls of a porous medium are replaced by a liquid surface? Experimental realizations of lubricant impregnated surfaces, like liquid-infused porous surfaces (SLIPS) or lubricant-impregnated surfaces (LIS) [13–17], have gained much attention in the recent years. These materials have outstanding properties for droplet manipulation due to their low friction, resistance to extreme conditions, and self-healing properties, as well as their ability to induce drag reduction in contact with a single liquid phase [18–20]. Here we address the fundamental question of how a liquid can spontaneously invade a porous medium coated with a liquid lubricant layer.

We show that the lubricant viscosity plays a determinant role to trigger a qualitative change in the dissipation mechanism where the liquid front advances at a constant rate, instead of slowing down, as would occur if the fluids were in direct contact with the solid. We also identify the high

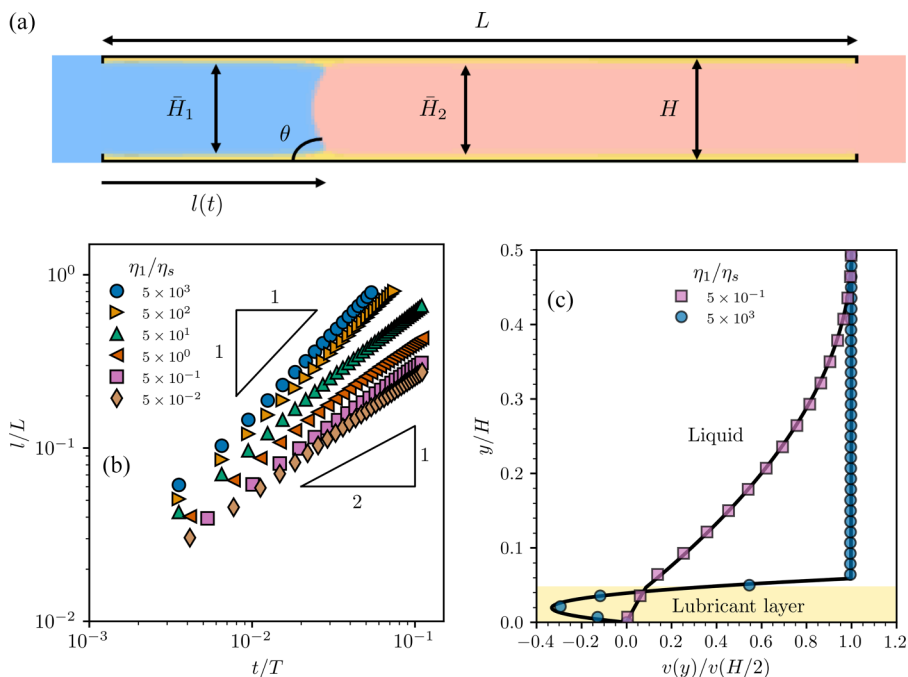


FIG. 1. Spontaneous imbibition in a lubricant coated channel. (a) Lattice-Boltzmann simulation snapshot. The liquid on the left, of width  $\bar{H}_1$ , preferentially wets the surface of a thin lubricant layer of width  $\bar{h}_1$ , and displaces a resident fluid in a channel of width  $H = \bar{H}_1 + 2\bar{h}_1$ , and length  $L$ . A meniscus, of apparent angle  $\theta$  and position  $l(t)$ , advances within the channel. (b) Effect of the viscosity of the lubricant,  $\eta_s$ , on the imbibition curves at fixed viscosity contrast between the displaced and displacing liquids,  $\eta_2/\eta_1 = 1 \times 10^{-2}$ . (c) Velocity profile in the displacing fluid and in the lubricant layer,  $v(y)$ , for  $\eta_1/\eta_s = 5 \times 10^{-1}$  (squares) and  $\eta_1/\eta_s = 5 \times 10^3$  (circles). The solid lines show the theoretical prediction (see text). The velocity is made dimensionless by the velocity at the center of the channel,  $v(H/2)$ , while the  $y$  coordinate is normalized by the channel width,  $H$ .

sensitivity of the liquid front to external perturbations, which opens an avenue to new modes of liquid manipulation at the microscale.

To study the front dynamics, we have carried out 2D lattice-Boltzmann (LB) numerical simulations of spontaneous imbibition into a solid channel coated with a liquid lubricant layer. We couple the LB method to a ternary free-energy model of three immiscible fluids, which we solve by using the Cahn-Hilliard equation. The ternary free-energy model [21] allows to independently choose the surface tensions of the liquids, and thus the Neumann angles at their intersection as well as the wettability of the solid. In our simulations, Fig. 1(a), two reservoirs hold liquids of equal density but different viscosities,  $\eta_1$  and  $\eta_2$ . The reservoirs are connected by a solid channel of length  $L$  and width  $H$ , whose internal surfaces are coated by a thin film of a third liquid of viscosity  $\eta_s$  (the lubricant). The lubricant is kept in place by two small pillars located at the edges of the channel. This geometry mimics SLIPS, where the lubricant is locked into the surface by roughness [22]. Furthermore, the lubricant wets the solid preferentially relative to the other two fluids, such that the spreading coefficients  $S_{1s} = \cos\theta_{1s} - \gamma_{1s} > 1$  and  $S_{s2} = \cos\theta_{s2} - \gamma_{s2} < -1$ . This effectively leads to a constant thickness of the lubricant layer, which remains attached to the solid due to the combination of the solid pillars that prevents the lubricant from going out of the channel, and the ability of the lubricant layer to wick the solid surface [23], as long as the capillary number remains small  $Ca = \eta_1 u / \gamma \ll 1$ , where  $\gamma$  the surface tension of the interface between liquids 1 and 2 and  $u$

the characteristic velocity of the front. Further details on the simulation methodology and choice of parameters are provided in the Supplemental Material [24].

As shown in the simulation snapshot of Fig. 1(a), an appropriate choice of the surface tensions leads to the spontaneous imbibition of liquid 1 into the channel, displacing liquid 2. The displacing and displaced liquids form an advancing meniscus with a well-defined apparent angle relative to the solid,  $\theta$ , suggesting a driving capillary force  $F_c \propto \gamma \cos \theta$ . Despite this similarity, the meniscus does not touch the solid, but moves on top of the lubricant layer.

We focus on the familiar case of a viscous liquid displacing a much less viscous fluid,  $\eta_2/\eta_1 = 10^{-2}$ , and analyze the motion of the meniscus at different lubricant viscosities,  $\eta_s$ . Figure 1(b) shows the corresponding  $l$  vs  $t$  curves, where the penetration length is normalized by the length of the tube, and time is normalized using the filling time predicted by Washburn's law,  $T = 3\eta_1 L^2/H\gamma \cos \theta$  [25]. For very large lubricant viscosity, the front advances following the scaling of Washburn's law,  $l(t) \sim t^{1/2}$ , indicating that the viscous force,  $F_v$ , increases with increasing  $l$ . Decreasing the lubricant viscosity leads to an unexpected result: The front grows linearly,  $l(t) \sim t$ , thus suggesting that  $F_v$  is independent of  $l$ . In addition, the filling time is significantly shorter than that predicted by Washburn's law. We shall show that these effects are not a transient due to inertia or dynamic-angle effects [25–28]. They correspond to a new long-time regime entirely dominated by the viscous dissipation in the lubricant film.

Figure 1(c) shows profiles of the tangential velocity of the displacing phase and the lubricant far upstream of the meniscus. The expected parabolic flow profile of a forced fluid [29] is approached for large  $\eta_s$ . The velocity in the lubricant layer becomes vanishingly small, which effectively behaves like a solid. In contrast, for small  $\eta_s$ , the flow profile resembles a plug flow in the displacing and displaced phases, while there is strong variation of the velocity in the lubricant layer, where shear stresses are sustained.

Building on these observations, we propose a simplified model of the flow in each fluid phase where we neglect the dynamics close to the meniscus and describe the flow profile in the four “bulk” flow regions depicted in Fig. 2(a). The tangential velocity profiles in the displacing and displaced phases,  $v_1(y)$  and  $v_2(y)$ , and in the adjacent regions of the lubricant layer,  $v_{s1}(y)$  and  $v_{s2}(y)$  are obtained from lubrication theory, assuming that the pressure profiles in each region, namely  $p_1$ ,  $p_2$ ,  $p_{s1}$ , and  $p_{s2}$ , only vary along the longitudinal coordinate  $x$ . Accordingly, the flow profiles are obtained by integrating the Stokes equations. Four out of the eight integration constants are found by imposing continuity of the velocity and tangential stress at the interface with the lubricant layer. The remaining constants are determined by fixing the average velocities of the fluids and the lubricant,  $\frac{1}{H/2-h} \int_h^{H/2} v_i dy = u$  and  $\frac{1}{h} \int_0^h v_{s_i} dy = u_s$  [24].

In general,  $u$  and  $u_s$  are independent free parameters; however, for the imbibition geometry the lubricant layer responds to the capillary driving force that acts on the meniscus. Therefore, we expect that if no external forces in the lubricant are present, the average velocity of the lubricant obeys  $u_s = \alpha u$ , with  $0 \leq \alpha \leq 1$ . This relationship allows us to eliminate the pressure gradient terms from the Stokes equations, and instead characterize the flow through  $u$  and  $\alpha$ . Figure 1(c) shows the excellent agreement of the theoretical prediction with the simulation velocity profiles, where  $u_s$  and  $u$  are fixed to the measured liquid flow. The theoretical results show that a vanishing average lubricant velocity  $u_s$  leads to a negative derivative of the velocity profile close to the solid, indicating a recirculating flow in the lubricant layer, as reported in SLIPS/LIS simulations [19] (see analytical solution in the Supplemental Material [24]).

The model can be used to determine the viscous friction force (per unit length) exerted by the lubricant layer on the moving fluids,  $F_v = 2l\tau_1 + 2(L-l)\tau_2$ , where  $\tau_i \equiv \eta_s dv_{s_i}(h)/dy$  is the shear stress. From the velocity profiles, we obtain [24]

$$F_v = \frac{4(2-3\alpha)u\eta_s}{h} \left( \frac{l}{1 + \frac{2\bar{H}}{3\delta_1 h}} + \frac{L-l}{1 + \frac{2\bar{H}}{3\delta_2 h}} \right). \quad (1)$$

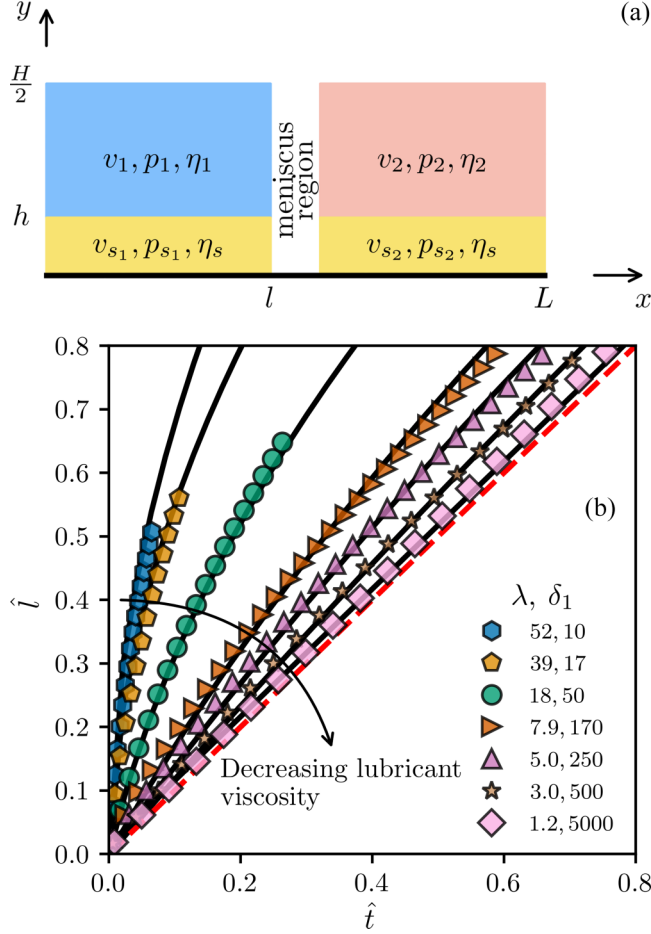


FIG. 2. (a) Schematics of the lubricant coated channel. The rectangular sections represent the bulk of the displacing and displaced liquids, and of the lubricant layer, which are separated by the meniscus region. (b) Theoretical imbibition curves (solid lines) vs simulation results (symbols) for different values of the parameter  $\lambda$ . For  $\lambda \rightarrow 1$ , corresponding to small lubricant viscosity, the imbibition curves approach the asymptotic limit  $\hat{l} = \hat{t}$  (red dashed line). The values of  $\Sigma$  with decreasing lubricant viscosity correspond to 0.03, 0.01, 0.2, 0.9, 1.7, 3.2, and 24, respectively.

Here,  $\bar{H}_i \equiv H - 2h = \bar{H}$  is the width of either liquid and  $\delta_i \equiv \eta_i/\eta_s$ ,  $i = 1, 2$  is the viscosity ratio between the displacing/displaced ( $i = 1/i = 2$ ) liquid and the lubricant. Letting  $\delta_i h/\bar{H} \rightarrow 0$ ,  $\eta_2/\eta_1 \rightarrow 0$  and setting  $\alpha = 0$ , this expression reduces to the classical result of the viscous force acting on a single liquid in contact with a solid channel, i.e.,  $F_v = 12\eta_1 ul/H$ . On the contrary, the limit of small lubricant viscosity is achieved by letting  $\delta_i h/\bar{H} \rightarrow \infty$ , where the friction force reduces to  $F_v = 4(2 - 3\alpha)\eta_s uL/h$ . In this regime the viscous force is dominated by the lubricant layer, despite being the less viscous phase, and the force does not depend on the position of the front; rather, its magnitude scales with the entire length of the channel,  $L$ . Comparing the energy dissipation rate in the bulk of the displacing and displaced liquids  $\dot{E}_b = \int_0^l \int_h^{H/2} \eta_1 |\nabla v_1|^2 dy dx + \int_l^L \int_h^{H/2} \eta_2 |\nabla v_2|^2 dy dx$ , to that of the lubricant  $\dot{E}_s = \int_0^l \int_0^h \eta_s |\nabla v_{s1}|^2 dy dx + \int_l^L \int_0^h \eta_s |\nabla v_{s2}|^2 dy dx$ , for  $\delta_i h/\bar{H} \rightarrow \infty$ , we find  $\dot{E}_b/\dot{E}_s \rightarrow 0$  [24]. Therefore, in this limit the energy dissipation occurs in the lubricant, and not in the bulk of the displacing and displaced phases.

The imbibition growth law,  $\hat{l}(t)$ , is derived from the force balance,  $F_c = F_v + F_m$ , between the capillary ( $F_c$ ), viscous ( $F_v$ ), and contact-line friction ( $F_m$ ) forces per unit length. The simulations show that the contact angle settles to a constant value  $\theta \approx \theta_e$  after a short transient. Accordingly,  $F_c = 2\bar{H}\gamma \cos \theta_e/H$ . The unbalanced interfacial stress close to the triple line is given by  $\gamma \cos \theta(u)$ . Since the contact angle is finite, for small velocities, one can expand this term  $\gamma \cos \theta(u) \simeq \gamma \cos \theta(0) + ku$ , resulting in  $F_m = ku$ , where  $k$  is a friction coefficient [25]. Independently, it has been reported that such a linear scaling holds in the limit  $\eta_s/\eta_1 \rightarrow 0$  [30]. The precise morphology of the meniscus, which determines the constant  $k$ , can have an impact on the front dynamics at early times, where the meniscus size is comparable to the penetration distance  $l(t)$ . However, we expect that at long times the friction in the bulk of the lubricant film will dominate over the friction in the meniscus. Therefore, the effect of the meniscus can be subsumed into  $F_m$ .

Using the dimensionless variables  $\hat{l} \equiv l/L$ ,  $\hat{t} \equiv t\gamma \cos \theta \bar{H}/LH[4\eta_s L(2 - 3\alpha)/h + k]$  and  $\hat{u} \equiv d\hat{l}/d\hat{t}$ , we can integrate the equation of the front motion and obtain

$$\frac{\hat{l}^2 (\lambda - 1)}{2 \left(1 + \frac{2\bar{H}}{3h\delta_1}\right)} + \hat{l} \left( \frac{1}{1 + \frac{2\bar{H}}{3h\delta_1}} + \lambda \Sigma \right) = \lambda(1 + \Sigma)\hat{t}, \quad (2)$$

where

$$\lambda \equiv \frac{\eta_1}{\eta_2} \frac{3\delta_2 h + 2\bar{H}}{3\delta_1 h + 2\bar{H}} \quad \text{and} \quad \Sigma \equiv \frac{kh}{4\eta_s L(2 - 3\alpha)}. \quad (3)$$

The parameter  $\lambda$  contains the relative effect of the viscosities of the three fluids together with the fraction of the channel occupied by the lubricant, and  $\Sigma$  quantifies the strength of the friction of the meniscus relative to the lubricant layer.

As shown in Fig. 2(a), Eq. (2) agrees well with the simulations, with the contact-line friction coefficient,  $k$ , used as the only fitting parameter [31]. The classical, diffusive-like growth regime of Washburn's Law is recovered by imposing  $\Sigma = 0$  and letting  $\delta_i h/\bar{H} \rightarrow 0$ . This eliminates the effect of the meniscus and reduces  $\lambda$  to the familiar viscosity contrast, i.e.,  $\lambda \rightarrow \eta_1/\eta_2$ . Then, taking  $\lambda \gg 1$  gives  $\hat{l} \rightarrow \sqrt{4\bar{H}\eta_s \hat{t}/3h\eta_1}$ .

On the other hand, for  $\delta_i h/\bar{H} \gg 1$  and  $\lambda \rightarrow 1$  Eq. (2) yields the linear growth law  $\hat{l} \rightarrow \hat{t}$ . After recovering dimensions, we find

$$l(t) = \frac{\bar{H}h\gamma \cos \theta}{H[4\eta_s L(2 - 3\alpha) + kh]} t. \quad (4)$$

Remarkably, the velocity of the front depends only on the viscosity and thickness of the lubricant layer and on the channel length.

The linear growth regime identified in this letter occurs for  $\delta_i h/\bar{H} \gg 1$ , where energy dissipation occurs primarily in the lubricant layer. For intermediate regimes, the asymptotic growth of the front will conform to Washburn's law. A crossover length  $l_c$  can be estimated by comparing the magnitudes of quadratic and linear contributions in Eq. (2). We obtain  $l_c \sim 2L(1 + \lambda\Sigma[1 + 2\bar{H}/3h\delta_1])/(\lambda - 1)$ , which implies  $l_c > L$  if  $\lambda < 3/(1 - 2\Sigma[1 + 2\bar{H}/3h\delta_1])$ . If the friction associated to the contact line is negligible compared to the lubricant dissipation  $\Sigma = 0$ , a crossover length  $l_c > L$  requires  $\lambda < 3$ . However, increasing the contact line friction increases the crossover length, and when  $\Sigma > 1/2$  Washburn's law will never be observed as the simulation results show in Fig. 2(b).

Here we have focused on the case of spontaneous imbibition. However, a low-viscosity lubricant layer has a strong impact in the sensitivity of the front to perturbations, and leads to a significant modification of the front dynamics when the fluids are subject to external forces. Let us consider a uniform external force acting on the displacing liquid,  $F_e = f\bar{H}l$ , for small  $\eta_s$ . Figure 3 shows a speed up of the front as it advances in the channel, in sharp contrast to the classical result of forced imbibition, where the motion of the front is linear. This effect is also captured by the theoretical

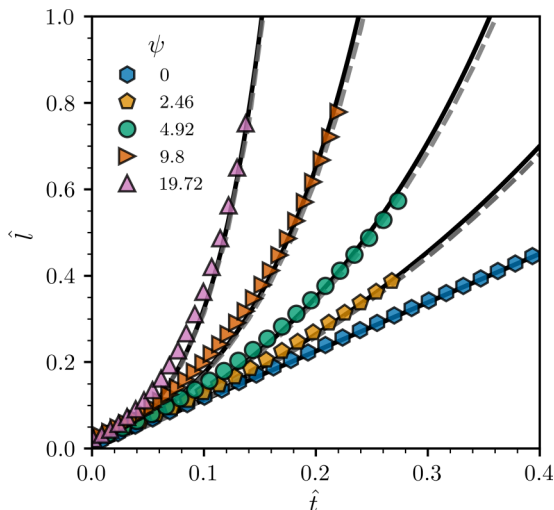


FIG. 3. Forced imbibition dynamics in a lubricant-coated channel. External forcing leads to an exponential growth of the position of the advancing front. The strength of the external force is quantified by the forcing coefficient  $\psi$ . The simulation parameters correspond to  $\Sigma = 24$ ,  $\lambda = 1.2$ , and  $\delta_1 = 5000$ . The symbols correspond to simulations, solid lines correspond to the numerical solution of the differential equation including the forcing term, and the dashed gray lines to the approximation in Eq. (5).

model upon adding an external force, which leads to the solid curves shown in Fig. 3 after numerical integration. An approximate expression of the growth law can be obtained in the regime  $\lambda \rightarrow 1$  and  $\delta_1 \rightarrow \infty$ , which gives

$$\hat{l} = \frac{e^{\psi \hat{t}} - 1}{\psi} = \frac{e^{t/t_i} - 1}{\psi}, \quad (5)$$

where  $\psi = LHf/2\gamma \cos \theta$  is the forcing coefficient. Equation (5) predicts an exponential invasion of the channel in agreement with the simulation results (dashed curved in Fig. 3), with a characteristic time scale  $t_i = \eta_s L/Hhf$  determined by the competition between viscous forces in the lubricant layer and the external forcing.

Our work can be used to design experimental setups that optimize imbibition in SLIPS/LIS channels. For example, using liquids with viscosities  $\eta_1 = 1700$  mPas,  $\eta_2 = 17$  mPas, and  $\eta_s = 10$  mPas [32], and a typical lubricant thickness of  $1 \mu\text{m}$  in a channel of  $H \simeq 20 \mu\text{m}$  would result in  $\lambda \simeq 8$ , thus making the linear regime reported here accessible in experiments. The analytical framework, validated with simulations, provides a starting point to characterize further effects that might be relevant in spontaneous imbibition processes in SLIPS and LIS, such as the precise role of the dissipation in the ridge, or the effect of the varying width of the lubricant in the channel.

Altogether, the ideas reported in this work will help rationalize the effect of a lubricant layer in naturally occurring situations as well as inspire solutions to technological challenges. For example, in pitcher plants, which inspired SLIPS originally [13], the textured surface that supports the lubricant layer has corrugations which form semiopen channels, and such structures could sustain the capillary flows reported in this paper [33]. Binary liquid capillary bridges, which spontaneously move in confinement and can therefore be used for droplet transport applications, have been reported to spontaneously leave a thin film of liquid adhered to a channel wall [34]. In antifouling applications [30,35–38], some studies suggest that bacteria can accumulate in the lubricant layer, limiting its medical applications [39]. Controlling spontaneous flows could be a key solution to enhance LIS properties and make it a suitable material for medical applications [40].

I.P. acknowledges support from the Ministerio de Ciencia, Innovación y Universidades (Grant No. PID2021-126570NB-100 AEI/FEDER-EU), from Generalitat de Catalunya under Program Icrea Acadèmia and Project 2021SGR-673. A.H.-M. acknowledges support from the Ministerio de Ciencia, Innovación y Universidades (Grant No. PID2022137994NB-100) and Generalitat de Catalunya (Grant No. 2021SGR00450).

- 
- [1] M. Rauscher and S. Dietrich, Wetting phenomena in nanofluidics, *Annu. Rev. Mater. Res.* **38**, 143 (2008).
  - [2] M. De Volder, S. J. Park, S. Tawfick, D. Vidaud, and A. J. Hart, Fabrication and electrical integration of robust carbon nanotube micropillars by self-directed elastocapillary densification, *J. Micromech. Microeng.* **21**, 045033 (2010).
  - [3] J. Bico, E. Reyssat, and B. Roman, Elastocapillarity: When surface tension deforms elastic solids, *Annu. Rev. Fluid Mech.* **50**, 629 (2018).
  - [4] Y. Snir and R. D. Kamien, Entropically driven helix formation, *Science* **307**, 1067 (2005).
  - [5] H. Hansen-Goos, R. Roth, K. Mecke, and S. Dietrich, Solvation of proteins: Linking thermodynamics to geometry, *Phys. Rev. Lett.* **99**, 128101 (2007).
  - [6] X. Li, D. R. Ballerini, and W. Shen, A perspective on paper-based microfluidics: Current status and future trends, *Biomicrofluidics* **6**, 011301 (2012).
  - [7] P. Estrela, K. Koczula, and A. Gallotta, Lateral flow assays, *Essays Biochem.* **60**, 111 (2016).
  - [8] E. W. Washburn, The dynamics of capillary flow, *Phys. Rev.* **17**, 273 (1921).
  - [9] M. Pradas and A. Hernández-Machado, Intrinsic versus superrough anomalous scaling in spontaneous imbibition, *Phys. Rev. E* **74**, 041608 (2006).
  - [10] M. Pradas, A. Hernández-Machado, and M. A. Rodríguez, Dynamical scaling of imbibition in columnar geometries, *Phys. Rev. E* **77**, 056305 (2008).
  - [11] M. Queralt-Martín, M. Pradas, R. Rodríguez-Trujillo, M. Arundell, E. Corvera Poiré, and A. Hernández-Machado, Pinning and avalanches in hydrophobic microchannels, *Phys. Rev. Lett.* **106**, 194501 (2011).
  - [12] B. K. Primkulov, J. Y. Y. Chui, A. A. Pahlavan, C. W. MacMinn, and R. Juanes, Characterizing dissipation in fluid-fluid displacement using constant-rate spontaneous imbibition, *Phys. Rev. Lett.* **125**, 174503 (2020).
  - [13] T.-S. Wong, S. H. Kang, S. K. Y. Tang, E. J. Smythe, B. D. Hatton, A. Grinthal, and J. Aizenberg, Bioinspired self-repairing slippery surfaces with pressure-stable omniphobicity, *Nature (London)* **477**, 443 (2011).
  - [14] J. D. Smith, R. Dhiman, S. Anand, E. Reza-Garduno, R. E. Cohen, G. H. McKinley, and K. K. Varanasi, Droplet mobility on lubricant-impregnated surfaces, *Soft Matter* **9**, 1772 (2013).
  - [15] D. F. Miranda, C. Urata, B. Masheder, G. J. Dunderdale, M. Yagihashi, and A. Hozumi, Physically and chemically stable ionic liquid-infused textured surfaces showing excellent dynamic omniphobicity, *APL Mater.* **2**, 056108 (2014).
  - [16] C. Urata, G. J. Dunderdale, M. W. England, and A. Hozumi, Self-lubricating organogels (SLUGs) with exceptional syneresis-induced anti-sticking properties against viscous emulsions and ices, *J. Mater. Chem. A* **3**, 12626 (2015).
  - [17] J. Cui, D. Daniel, A. Grinthal, K. Lin, and J. Aizenberg, Dynamic polymer systems with self-regulated secretion for the control of surface properties and material healing, *Nat. Mater.* **14**, 790 (2015).
  - [18] S. Kim, H. N. Kim, and S. Lee, A lubricant-infused slip surface for drag reduction, *Phys. Fluids* **32**, 091901 (2020).
  - [19] C. Vega-Sánchez, S. Peppou-Chapman, L. Zhu, and C. Neto, Nanobubbles explain the large slip observed on lubricant-infused surfaces, *Nat. Commun.* **13**, 351 (2022).
  - [20] P. A. Tsai, Slippery interfaces for drag reduction, *J. Fluid Mech.* **736**, 1 (2013).
  - [21] C. Semperebon, T. Krüger, and H. Kusumaatmaja, Ternary free-energy lattice Boltzmann model with tunable surface tensions and contact angles, *Phys. Rev. E* **93**, 033305 (2016).

- [22] N. Gheraldi, J. Guan, L. Dodd, P. Maiello, B. Xu, D. Wood, M. Newton, G. Wells, and G. Mchale, Double-sided slippery liquid-infused porous materials using conformable mesh, *Sci. Rep.* **9**, 13280 (2019).
- [23] J. S. Wexler, I. Jacobi, and H. A. Stone, Shear-driven failure of liquid-infused surfaces, *Phys. Rev. Lett.* **114**, 168301 (2015).
- [24] See Supplemental Material at <http://link.aps.org/supplemental/10.1103/PhysRevFluids.9.L072002> for further information on the model.
- [25] É. Ruiz-Gutiérrez, S. Armstrong, S. Lévêque, C. Michel, I. Pagonabarraga, G. G. Wells, A. Hernández-Machado, and R. Ledesma-Aguilar, The long cross-over dynamics of capillary imbibition, *J. Fluid Mech.* **939**, A39 (2022).
- [26] P. Joos, P. Van Remoortere, and M. Bracke, The kinetics of wetting in a capillary, *J. Colloid Interface Sci.* **136**, 189 (1990).
- [27] G. Martic, J. De Coninck, and T. Blake, Influence of the dynamic contact angle on the characterization of porous media, *J. Colloid Interface Sci.* **263**, 213 (2003).
- [28] D. Quéré, Inertial capillarity, *Europhys. Lett.* **39**, 533 (1997).
- [29] H. Bruus, *Theoretical Microfluidics*, Oxford Master Series in Physics (Oxford University Press, Oxford, 2008).
- [30] A. Keiser, L. Keiser, C. Clanet, and D. Quéré, Drop friction on liquid-infused materials, *Soft Matter* **13**, 6981 (2017).
- [31] The value of  $k = 34$  simulation units, is computed once, which indicates it has a weak dependence on the lubricant properties and is controlled by the viscosities in the displacing and displaced fluids.
- [32] S. Peppou-Chapman, J. K. Hong, A. Waterhouse, and C. Neto, Life and death of liquid-infused surfaces: A review on the choice, analysis and fate of the infused liquid layer, *Chem. Soc. Rev.* **49**, 3688 (2020).
- [33] H. F. Bohn and W. Federle, Insect aquaplaning: *Nepenthes* pitcher plants capture prey with the peristome, a fully wettable water-lubricated anisotropic surface, *Proc. Natl. Acad. Sci.* **101**, 14138 (2004).
- [34] J. Bico and D. Quéré, Self-propelling slugs, *J. Fluid Mech.* **467**, 101 (2002).
- [35] M. Kratochvil, M. Welsh, U. Manna, B. Ortiz, H. Blackwell, and D. Lynn, Slippery liquid-infused porous surfaces that prevent bacterial surface fouling and inhibit virulence phenotypes in surrounding planktonic cells, *ACS Infectious Diseases* **2**, 509 (2016).
- [36] M.-S. Lee, H. Hussein, S.-W. Chang, C.-Y. Chang, Y.-Y. Lin, Y. Chien, Y.-P. Yang, C.-Y. Chen, S.-H. Chiou, R. Jih, R. Hwu, V. Charushin, S. Bachurin, M.-S. Lee, H. Hussein, S.-W. Chang, C.-Y. Chang, Y.-Y. Lin, and C.-C. Chang, International journal of molecular sciences nature-inspired surface structures design for antimicrobial applications, *Int. J. Mol. Sci.* **24**, 1348 (2023).
- [37] Y. Yang, Q. Zhu, L. Xu, and X. Zhang, Bioinspired liquid-infused surface for biomedical and biosensing applications, *Front. Bioeng. Biotechnol.* **10**, 1032640 (2022).
- [38] Y. Xie, J. Li, D. Bu, X. Xie, X. He, L. Wang, and Z. Zhou, *Nepenthes*-inspired multifunctional nanoblades with mechanical bactericidal, self-cleaning and insect anti-adhesive characteristics, *RSC Adv.* **9**, 27904 (2019).
- [39] J.-U. Jeong, Y.-G. Heo, J.-A. Cho, Y. Roh, S. J. Kim, C.-H. Lee, and J.-W. Lee, Nanostructure-based wettability modification of TiAl6V4 alloy surface for modulating biofilm production: Superhydrophilic, superhydrophobic, and slippery surfaces, *J. Alloys Compd.* **923**, 166492 (2022).
- [40] Y. Zhu, G. Mchale, J. Dawson, S. Armstrong, G. Wells, R. Han, H. Liu, W. Vollmer, P. Stoodley, N. Jakubovics, and J. Chen, Slippery liquid-like solid surfaces with promising antibiofilm performance under both static and flow conditions, *ACS Appl. Mater. Interfaces* **14**, 6307 (2022).